High-resolution quantum-beat and rf resonance spectroscopy after grazing-ion–surface scattering and its application in studies of the hyperfine structure of stable terms in ^{14}N I, II, and III

A. Schirmacher* and H. Winter
Institut für Kernphysik der Universität Münster, Wilhelm-Klemm-Strasse 9, D-4400 Münster, Federal Republic of Germany
(Received 21 July 1992)

High-resolution spectroscopy studies of hyperfine structures of stable terms in ^{14}N I, II, and III by quantum-beat and rf resonance spectroscopy after grazing-ion–surface scattering are reported on. From the data, the electric quadrupole moment of the ^{14}N nucleus $Q=20.0\pm0.2$ mb and the quadrupole coupling constants eQq_{at}/h of ^{14}N atoms in $2p$ and $2p^2$ configurations have been deduced. Extrapolation yields $eQq_{at}/h=11.2\pm0.2$ MHz for a single electron in the ground term of the $2p^3$ configuration of the neutral atom.

PACS number(s): 32.30.Bv, 21.10.Ky, 35.10.Di, 35.10.Fk

I. INTRODUCTION

The spectroscopy of hyperfine (hf) splittings of electronic terms in free atoms and ions provides the basis for experimental tests of atomic structure calculations, studies of hf interaction, and in particular the determination of nuclear properties. As a consequence, magnetic dipole and electric quadrupole moments of many nuclei have been deduced from data obtained by atomic spectroscopy. In this paper a detailed report is given on hf studies of (meta) stable terms in ^{14}N atoms and ions using two different techniques. By extending quantum-beat and radio-frequency (rf) resonance methods in fast ion-beam spectroscopy we have established procedures to investigate the hf structures of stable atomic terms. The application of these techniques results in the resolution of the hf splittings of most of the stable terms of ^{14}N I, II, III. Our measurements represent the consequent studies of these structures. Since the quadrupole interaction in ^{14}N I $2p^3$ atoms is small, the data on hf splittings in ^{14}N II and ^{14}N III are of relevance for determining the electric quadrupole moment of the ^{14}N nucleus $Q(^{14}\mathrm{N})$ and the quadrupole coupling constants of ^{14}N atoms in $2p^n$ configurations ($n=1, 2, 3$).

II. EXPERIMENTAL METHODS

The main feature of our experiments is the preparation of stable electronic terms of atoms and ions by scattering fast ions from a solid surface under grazing-incidence conditions. In this extreme geometry of ion-surface collisions, the low symmetry of the interaction processes is characterized by three vectors: the surface normal $\mathbf{y}$ and the velocity vectors $\mathbf{v}_{pi}$ and $\mathbf{v}_{po}$ of the incoming and outgoing projectiles. The trajectories of projectiles are given by two vastly different velocity (and time) scales, i.e., a fast motion with $v_{\parallel}\approx v_p$ parallel to the surface and a slow perpendicular motion $v_{\perp}=v_p\sin\phi_{in}\ll v_p$ (ϕ_{in} is the grazing angle of incidence). As a consequence, projectile ions interact only with the topmost atomic layer of the (ideal) surface in a sequence of soft quasielastic small-angle collisions ($\mathbf{v}_{pi}\approx\mathbf{v}_{po}$), so that projectiles are specularly reflected at the surface with well-defined angular and energy distributions. A second relevant feature of grazing-ion–surface collisions is a large vector polarization of orbital angular momenta associated with atomic terms in an ensemble of scattered atoms. This anisotropy has been found in many ion-target combinations where generally an orientation $P_L=\langle L_z\rangle/L>0.5$ of orbital angular momenta L is observed [1] (the axis of quantization is chosen along $-\mathbf{y}\times\mathbf{v}_p$). P_L can be probed directly by investigating the emission of polarized light from excited atomic terms, where P_L is in good approximation proportional to the degree of circular polarization fraction given by the normalized Stokes parameter $S/I=[I(\sigma^-)-I(\sigma^+)]/[I(\sigma^-)+I(\sigma^+)]$; $I(\sigma^{\pm})$ are the intensities of light with negative and positive helicities, respectively. In experiments S/I of up to 96% has been observed after the excitation of atoms by grazing surface collisions [2]. Through spin-orbit and hyperfine interactions, part of the atomic orientation P_L is transferred into the electronic and nuclear spin ensembles with spins S and I, respectively. Since, for light atoms, the times of formation of electronic terms ($\approx10^{-14}$ s) are generally smaller than corresponding inverse fine- and hf-interaction frequencies, the transient transfer of anisotropy is well separated from the excitation process. This transfer leads to nonzero spin polarizations $P_S=\langle S_z\rangle/S$ and $P_I=\langle I_z\rangle/I$. The transfer of collision-induced anisotropy $P_L(t=0)$ to the nuclear spin ensemble (P_I) via fine and hf interaction is described by [3]

$$P_I(t)=\frac{L(I+1)}{I(L+1)}P_L(t=0)\frac{\sum_{J,F_1,F_2}A^1\cos\omega_{JF_1F_2}t}{\sum_{J,F_1,F_2}A^0}\ , \qquad (1)$$

with

 ©1993 The American Physical Society

$$A^k=(-1)^{L+S+k+3J+2I+F_1+F_2}\times\frac{(2J+1)(2F_1+1)(2F_2+1)}{(2I+1)(2S+1)}\times\begin{Bmatrix}J & J & k\\ L & L & S\end{Bmatrix}\begin{Bmatrix}F_1 & F_2 & k\\ J & J & I\end{Bmatrix}\begin{Bmatrix}F_1 & F_2 & k\\ I & I & J\end{Bmatrix}, \quad (2)$$

where, assuming LS coupling, the quantum numbers L, S, J, I, and F denote atomic $|LSJIF\rangle$ terms with total angular momenta F and $\omega_{JF_1F_2}=\omega_{JF_1}-\omega_{JF_2}$ hyperfine-interaction frequencies. With times of integration $\Delta T\gg 1/\omega_{JF_1F_2}$ terms with $F_1\neq F_2$ average out in the sum of the denominator in Eq. (1), and one obtains a constant nuclear polarization $P_I=\langle P_I(t)\rangle_t$. This condition is generally met in experiments of grazing-ion–surface collisions to obtain nuclear spin polarized fast beams [4] where solid targets of lengths $\Delta x\gg v/\omega_{JF_1F_2}$ are used (v is the projectile velocity). In those experiments it is crucial to have stable atomic terms with nonzero orbital angular momenta to obtain $P_L\neq 0$. Depending on the atomic electronic structure and nuclear spin, P_I of up to 25% is observed with this technique at projectile energies between several kilo-electron volts and mega-electron volts [5].

In those studies the detection of P_I is performed using an "optical method" [4], since the projectile energies used are generally too low to apply standard methods of nuclear physics. The interaction of the fast nuclear spin polarized beam with thin solid foils ("beam-foil excitation") yields excited atomic terms. Since symmetry of the foil excitation at $t'=0$ postulates $P_L'(t'=0)=0$, and since P_I is not affected by this interaction, the retransfer of anisotropy from the nuclear spin ensemble to the electronic shell yields $P_L'(t'>0)\neq 0$, which serves as a direct measure for P_I at $t'=0$. Observation of the degree of circularly polarized light S/I emitted after foil excitation allows $P_I=\alpha^{-1}S/I$ to be determined, where the "analyzing power" α is determined by properties of the atomic transition (angular momenta, lifetime and hf interaction of the upper term, etc.) and of the detection geometry. For the work reported here, a precise knowledge of α is not needed, since relative variations of P_I contain the relevant information. As a consequence, in most of our experiments we average over a number of spectral lines ("broadband detection") without specifying individual contributions of terms in detail.

Based on the property of grazing-ion–surface scattering to populate ensembles of stable terms in atoms and ions with large polarization, and detecting P_I by an "optical" beam-foil method, we have applied these features to measure hf splittings of stable terms using two different methods.

(I) Recording the transient transfer of anisotropy between nuclear spin and electronic ensembles of free atoms and/or ions after surface scattering via $P_I(t)$ yields a modulation (quantum beats) according to the hf splittings of relevant atomic terms [see Eq. (1)].

(II) Modification of P_I after surface scattering due to $M1$ transitions between hf levels of atoms or ions induced by a resonant rf field allows the hf splittings of stable terms to be deduced.

In two separate sections we will outline the method, experiment, and results of both techniques in some detail. Before this we will describe a technique which allows the terms that are preferentially populated after surface scattering to be identified. This information is essential for the application of the two methods.

III. "ZEEMAN QUANTUM BEATS" AFTER GRAZING-ION–SURFACE SCATTERING

The two techniques reported here allow hf splittings of stable atomic terms to be resolved. However, the schemes of detection do not provide unambiguous information on the terms that contribute to the signals. Since the population of atomic terms after grazing surface scattering was unknown until now and their hf splittings have not been resolved before, information on the relative contributions of stable terms in our experiments is relevant. Andrä and Winter [3] demonstrated the feasibility of the quantum-beat method (method I). The lack of information on the population of atomic terms has led, however, to an incorrect term assignment of the measured hf splittings. In order to investigate the contributions of possible (meta) stable atomic terms, in a drift zone between target and detection, we have applied an additional longitudinal magnetic field H_X. In this field the total angular momenta of levels $|(\gamma LS)JIF\rangle$ precess because of their associated magnetic momenta $\boldsymbol{\mu}=g_F\mu_B\mathbf{F}$ (μ_B is the Bohr magneton) around the H_X direction (beam axis). By using a target length $\Delta x\gg v/\omega_{JF_1F_2}$, with Eqs. (1) and (2) we obtain

$$S/I=\alpha\langle P_I(t)\rangle=\alpha\sum_{\gamma,L,S}\sigma_{\gamma LS}\,{}^{\gamma LS}P_I(H_X)=\alpha\sum_{\gamma,L,S}\sigma_{\gamma LS}\frac{L(I+1)}{I(L+1)}\,{}^{\gamma LS}P_L\times\sum_{J,F}A_{JF}\cos[g_F(\mu_B/\hbar)\Delta T_H H_X], \quad (3)$$

where $A_{JF}=A^1/\sum A^0$ are transfer coefficients ($F=F_1=F_2$), ΔT_H the interaction time with the magnetic field H_x, and $\sigma_{\gamma LS}$ and ${}^{\gamma LS}P_L$ the populations and orientations, respectively, of LS terms. g_F denotes the g_F factors of $(LS)JIF$ terms which generally differ for different times. In Table I the g_F factors and coefficients A_{JF} are listed for stable terms in ^{14}N I $2p^3\,{}^4S,{}^2P,{}^2D$. It is evident from the table that the g_F spectrum can be considered as a "fingerprint" for a term.

In our experiments we thus obtain information on the contribution of atomic terms to the overall nuclear polarization P_I by recording the modulation in S/I due to a variation of $T_H H_X$ [see Eq. (3)]. No information is obtained for terms with $L=0$. From the modulation amplitudes we deduce $\sigma_{\gamma LS}\,{}^{\gamma LS}P_L$, i.e., the product of population and anisotropy of LS terms. In conclusion, the application of a longitudinal magnetic field induces selectivity with respect to atomic terms in our method of

TABLE I. Factors for the transfer of orientation from the ensemble of the atomic orbital angular momenta to the nuclear spin system; the electronic and nuclear spins are assumed to be unpolarized at the instant of the excitation process.

Term	L	J	F_1	F_2	g_J	g_F	Transfer factor
^4S	0	1.5	0.5	0.5	2.0	3.333	0
	0	1.5	1.5	0.5	2.0		0
	0	1.5	1.5	1.5	2.0	1.466	0
	0	1.5	2.5	1.5	2.0		0
	0	1.5	2.5	2.5	2.0	1.200	0
^2D	2.0	1.5	0.5	0.5	0.8	1.333	−0.019 245
	2.0	1.5	1.5	0.5	0.8		−0.076 980
	2.0	1.5	1.5	1.5	0.8	0.587	0.033 871
	2.0	1.5	2.5	1.5	0.8		−0.083 138
	2.0	1.5	2.5	2.5	0.8	0.480	0.145 492
	2.0	2.5	1.5	1.5	1.2	1.680	−0.064 663
	2.0	2.5	2.5	1.5	1.2		−0.086 218
	2.0	2.5	2.5	2.5	1.2	1.060	0.040 909
	2.0	2.5	3.5	2.5	1.2		−0.087 977
	2.0	2.5	3.5	3.5	1.2	0.857	0.197 949
^2P	1.0	0.5	0.5	0.5	0.666	−0.222	−0.024 691
	1.0	0.5	1.5	0.5	0.666		−0.098 765
	1.0	0.5	1.5	1.5	0.666	0.222	0.123 457
	1.0	1.5	0.5	0.5	1.333	2.222	−0.030 864
	1.0	1.5	1.5	0.5	1.333		−0.123 457
	1.0	1.5	1.5	1.5	1.333	0.978	0.054 321
	1.0	1.5	2.5	1.5	1.333		−0.133 333
	1.0	1.5	2.5	2.5	1.333	0.800	0.233 333

detection, thus achieving unambiguous assignment of measured hf splittings to atomic terms in our studies.

A. Experimental setup

The experimental setup for our "Zeeman quantum-beat" studies is sketched in Fig. 1. This setup was also used for the rf resonance experiments (method II) which will be discussed in Sec. V. The target—a thin, highly polished Si(111) wafer of 4 in. diameter—is positioned by a manipulator in a UHV chamber at a base pressure of about 10^{-10} mbar. Differential pumping stages on both ends of the chamber with slits of 0.7×10 mm^2 provide sufficient isolation against the pressures in the beam line and the section of detection (typically 10^{-7}–10^{-6} mbar). The slits provide a good collimation of the projectile beam (divergence about 1 mrad). The first pumping stage contains electric field plates to deflect eventually the projectile beam, and field plates are used in the other stage to separate the charge states of the scattered beam. About 1 m behind the target a coaxial rf transmission line of 4.0 m in length was installed (details are given in Sec. V). This line consists of two coaxial copper tubes with a 6.5-mm spacing for the passage of the scattered projectiles. Earth and stray magnetic fields in the line are reduced over the total length by a coil consisting of 735 windings of a 5-mm copper strip, and an additional coaxial μ-metal shield.

In our "Zeeman beat" studies we made use of the coil to generate a longitudinal magnetic field; a current of 2.2 A results in a magnetic field of about 5 G. A system of magnetic coils 1.5 m in diameter centered at the target and directed along the Earth magnetic field provides a field compensation in the drift zone between the target and the transmission line. The transmission line is mounted in a vacuum tube (50 mm inner diameter) which is connected at both ends to vacuum chambers pumped by turbo pumps and liquid-nitrogen cold shields to a pressure of some 10^{-7} mbar. The chamber at the end of the beam line contains a Faraday cup and thin carbon foils (≈5 μg/cm^{-2}) in a holder which is mounted on a linear motion feedthrough. These foils (circular hole 6 mm in diameter) are used to excite a fraction of transmitted atoms to monitor the nuclear orientation P_I of the beam [4] by means of an "optical method."

The detection of circularly polarized light after foil excitation is performed along z (axis of quantization) with a quarter wave plate in front of a linear polarization 90° beam splitter and two cooled RCA Model 31034-A02 photomultipliers. The emitted light is collected by a fused quartz lens ($f=50$ mm) covering a solid angle of detection of $0.04\times4\pi$ sr. This setup of detection allows a simultaneous measurement of the intensities $I(\sigma^-)$ and

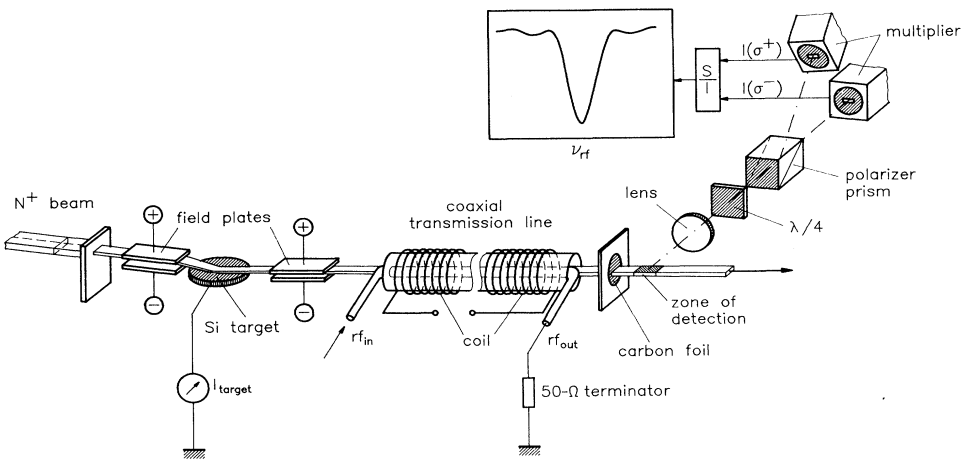

FIG. 1. Sketch of the experimental setup for Zeeman-beat and rf resonance studies. Magnetic coils shielding the drift zone are not shown.

$I(\sigma^+)$, so that fluctuations in the ion-beam current affect the normalized quantity S/I only minimally. Since the variation of S/I in our rf experiments (see Sec. V) turned out to be extremely small, this detection method is a basic prerequisite to successfully carrying out such an investigation.

B. Experiments and results

The experiments start with an adjustment of the Si target in the UHV chamber, which is dictated by a compromise in intensity and quality with respect to the angular and energetic spread of the scattered beam. We found grazing angles of incidence Φ_{in} and exit Φ_{out} of a few 0.1° to be a good choice. Information on the target position and the angular spread of the beam is obtained by scanning a thin wire (0.1 mm diameter) through the scattered beam. This wire is directed parallel to the z axis at a distance of 0.8 m behind the target, and the current (primarily due to kinetic electron emission) serves as a signal to monitor the intensity of the beam.

Figure 2 shows as an example the angular distribution after the scattering of 300-keV N^+ ions from a Si(111) surface. A fraction of the beam passes over the target without interaction and serves as a reference for the direction of the projectile beam (see inset of figure). The distribution in Fig. 2 represents a well-defined scattered beam with an angular full width at half maximum (FWHM) of about 0.4°. For the experiments a portion of scattered projectiles as given by the dashed part in the figure is used. The peaks of the distributions of direct and scattered beams determine the most probable angle of scattering $\Phi_S = 0.6°$, i.e., $\Phi_{in} \approx \Phi_{out} \approx 0.3°$ for the specularly reflected fraction of the beam. Energy loss and straggling of the scattered projectiles amounts to about 1.5% (see Sec. IV).

Since our studies will focus on hf interactions in atoms of different charge states, the distribution of charge states after ion-surface scattering is important information. In Fig. 3 the fractions of charge states as a function of energy for $^{14}N^+$ ions interacting with the Si(111) surface are shown. The different charge states are analyzed by

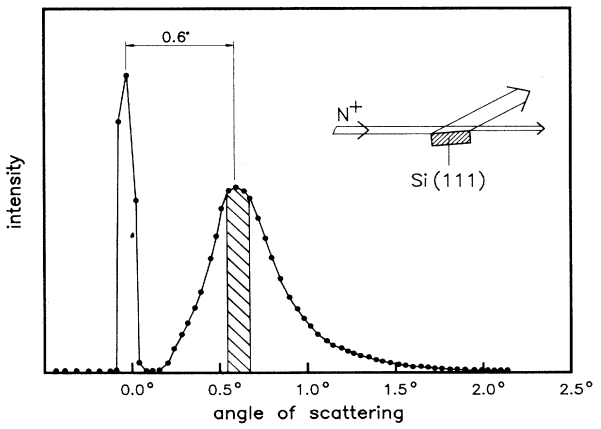

FIG. 2. Scattering distribution after the interaction of 300-keV N^+ ions scattered from a Si(111) surface.

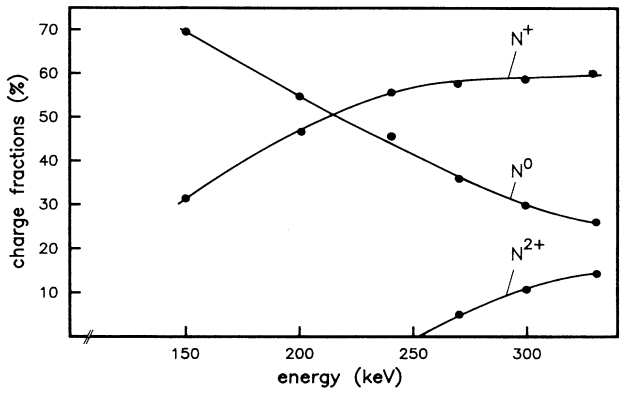

FIG. 3. Charge state fractions in a nitrogen beam after scattering of $^{14}N^+$ ions from a Si surface ($\Phi_{in} \approx \Phi_{out} \approx 0.4°$) as a function of projectile energy

means of electric field plates in the second pumping stage. As the data show a pronounced dependence on energy, the proper choice of projectile energy is relevant to optimize the contributions of atoms in corresponding charges states. Energies below about 150 keV are favorable for investigating atomic terms in neutral ^{14}N I, and for studies in ^{14}N III energies larger than about 300 keV.

We start the "Zeeman beat" experiments with an investigation of the neutral fraction of the scattered beam which is separated by applying a high voltage to the plates between the target and the wave guide. The wave guide and the detecting device are adjusted in such a way that the neutral fraction of the beam is transmitted through the carbon foil. In order to obtain an oscillatory signal in S/I [see Eq. (3)], we keep the interaction time with the magnetic field ΔT_H fixed and vary the strength of the longitudinal field H_X. To identify the contributions of various atomic terms by their g_F spectra a sufficient number of periods of oscillations must be observed; i.e., $g_F(\mu_B/\hbar)\Delta T_H H_X \gg 1$. Since we also have to keep $g_F(\mu_B/\hbar)H_x \ll \omega_{JF_1F_2}$ to maintain defined g_F factors ($H_X < 10$ G), ΔT_H must be sufficiently long. This condition is met by the length of the region of interaction with the magnetic field (2.2 or 4.0 m). The interaction time of 100-keV ^{14}N projectiles with the field is 1.9 or 3.4 μs.

In Fig. 4 the dependence of S/I on the magnetic field H_X for 100-keV neutral ^{14}N atoms is displayed. The curve shows a complex oscillatory structure, and its Fourier transform given in Fig. 5 is referred directly to g_F factors. A comparison of Fig. 5 with Table I shows the dominant contribution of the ^2D term; the complete g_F factor spectrum of this term is clearly resolved, and the relative intensities of the components are reproduced reasonably well by the factors A_{JF} in Eq. (3). The spectrum in Fig. 5 reveals only a small contribution of ^2P. This selective population of ^{14}N I ^2D is interpreted in terms of a model of the consecutive capture of $2p$ electrons with a large orientation of orbital angular momenta [6].

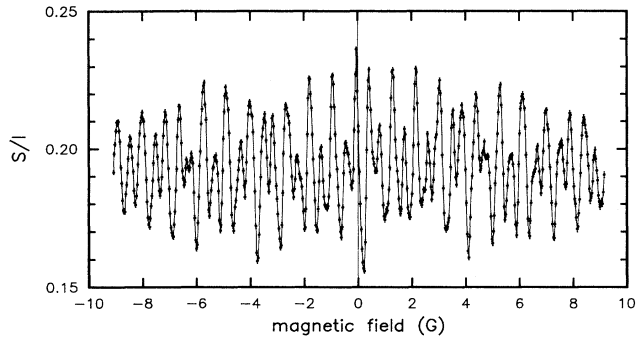

FIG. 4. Zeeman-beat oscillations in the nuclear orientation $P_I \sim S/I$ of the neutral charge state fraction after the interaction of 100-keV N^+ projectiles with a Si surface (maximum magnetic field, ± 9.2 G; solid line is a guide to the eye).

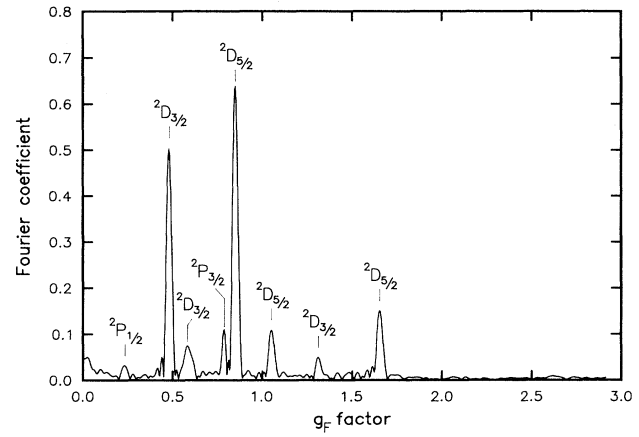

FIG. 5. Fourier transform of the data shown in Fig. 4. All hf levels in ^{14}N I $^2D_{3/2,5/2}$ and two levels in $^2P_{3/2,1/2}$ are identified by their g_F factors.

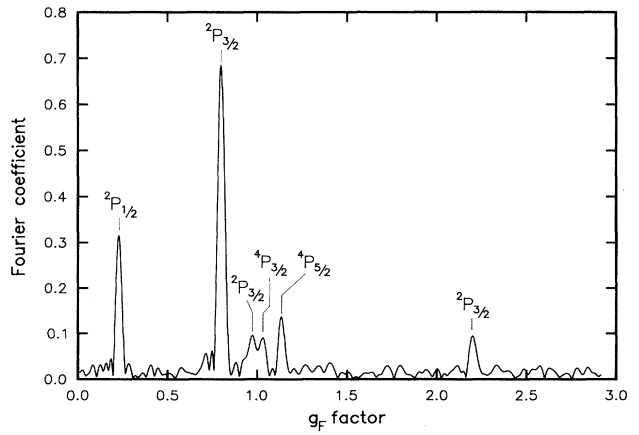

FIG. 6. Fourier transform of a Zeeman-beat measurement in N III ($E_{in}=320$ keV).

Our investigations of ^{14}N II result in comparable contributions of ^{14}N II $2p^2\,{}^3P$ and ^{14}N II $2p^2\,{}^1D$. Figure 6 shows a Fourier spectrum obtained after separation of ^{14}N III at a projectile energy of 320 keV. The data show a dominant contribution of the ^{14}N III $2p\,{}^2P$ term, whereas ^{14}N III $2s2p^3\,{}^4P$ is only weakly populated.

In summarizing the "Zeeman beat" experiments, we have identified the stable atomic terms in the scattered beam which are relevant to our hf studies outlined in Secs. IV and V: ^{14}N I ^2D, ^{14}N II ^3P and ^1D, ^{14}N III ^2P. It turns out that all hf splittings observed in our studies can be unambiguously ascribed to those terms.

IV. ZERO-FIELD QUANTUM BEATS IN STABLE ATOMIC TERMS

After grazing scattering of fast ions from surfaces, well-defined beams are obtained. The monoenergetic motion of atoms and ions with velocity $v=\Delta x/\Delta t$ allows us to profit from a unique feature of fast-beam spectroscopy: time resolution in the subnanosecond regime ($v \approx$ mm/ns) by an observation in geometrical translation along the beam axis [7,8]. Knowledge of the ion velocity v allows the transformation from length to time scales. To resolve hf-interaction frequencies, the transient transfer of anisotropy between electronic shell and nuclear spin ensembles after surface scattering is observed. Taking into account the finite length δx of the target, i.e., the definition of the interval of time of excitation $\delta T=\delta x/v$, from Eq. (1) we have

$$P_I(x)=\frac{L(I+1)}{I(L+1)}P_L \times \frac{\sum_{J,F_1,F_2} A^1 R_{ex}(\omega_{JF_1F_2},\delta x)\cos(\omega_{JF_1F_2}x/v)}{\sum_{J,F_1,F_2} A^0}, \tag{4}$$

where R_{ex} is given by

$$R_{ex}(\omega,\delta x)=\sin(\omega\delta x/2v)/(\omega\delta x/2v)\ . \tag{5}$$

Thus the finite length of the zone of excitation reduces the amplitudes of the modulation signal by a factor R_{ex}. R_{ex} can be considered to be the frequency response of the "quantum-beat spectrometer." An inspection of Eq. (5) shows that rather high frequencies are observable, but at the cost of a reduction in signal amplitude. Assuming a linear dependence of beam intensity I on δx, optimization based on a figure of merit $R_{ex}I^{1/2}$ results in $\delta x \approx 2.33v/\omega$. In our studies we expect frequencies between about 10 and 500 MHz, therefore at beam velocities of about mm/ns, δx should be chosen in the millimeter domain.

The frequency response of detection R_{det} is given by the geometrical extension of the foil along the beam axis (or better still, the surface at the entrance side of the foil). The definition of the position of detection is therefore of the order of microns, and $R_{det}=1$ can be assumed throughout our studies.

A. Experimental setup

A sketch of the experimental setup and procedure is shown in Fig. 7. The setup is similar to the one used in studies by Andrä and Winter [3] to demonstrate the feasibility of the method. However, quite a number of conceptual and experimental improvements have been introduced. The experiment is performed in a vacuum chamber at a base pressure of a few 10^{-7} mbar obtained by a turbo pump and a cold shield kept at liquid-nitrogen temperature. $^{14}N^{+}$ or (in a few cases) $^{14}N_2{}^{+}$ beams with current densities up to 10 μA/mm^2 and energies ranging from about 50 keV to 1 MeV are well collimated by a set of slits (0.8×8 mm^2 and 0.1×8 mm^2, 270 mm apart) and bent onto the target surface by means of electric field plates. The target is cut from a Si(111) wafer rectangular in shape and 15 mm in width; target lengths between $\delta x = 2$ and 5 mm are used in various experimental runs.

Grazing angles of incidence $\Phi_{in} \approx 0.5°$ are chosen in our studies by bending the projectile beam and tilting the target so that the specularly reflected fraction of the beam is parallel to the axis of the beam line. This adjustment is performed from outside the vacuum chamber by a flexible feedthrough. The specular fraction of the scattered beam is selected by a slit (0.3×10 mm^2) about 45 mm behind the target. The position of this slit is adjusted in height with the beam on target. A second pair of electric field plates (25 mm long) is positioned behind the target and can be used to isolate a charge state in the scattered beam. Slits, field plates, and target are mounted on a carriage which can be translated precisely parallel to the beam axis via stepmotor control. With this drive the distance between the target and the carbon foil of the detecting device can be varied to record the transient transfer of anisotropy due to hf interaction. The detection system used in this setup is comparable with the one described in Sec. III A.

The exit side of the vacuum chamber is equipped with an energy analyzer to determine the actual energy (velocity) of the scattered beam. The electrostatic 90° cylindrical energy analyzer 500 mm in radius has an energy resolution better than 10^{-3} and is calibrated by two different techniques: (1) zero-field quantum beats of the 658-MHz fine structure in He I $3p\ ^3P$ ($J=2$, $J'=1$) after beam-foil excitation [9] and (2) dissociation of molecules in a gas target kept at a high voltage [10]. Both calibration procedures result in correction factors 0.985±0.002 for the energy deduced from the geometry of the analyzer.

B. Experiments and results

In our quantum-beat experiments we vary the distance between target and detection by a translation of the target in equidistant steps and simultaneously record $I(\sigma^-)$ and $I(\sigma^+)$. In Fig. 8, data after the interaction of 300-keV $^{14}N^{+}$ ions at $\Phi_{in} \approx 0.5°$ with a Si(111) surface of length $\delta x = 4.4$ mm are shown. The geometry of the setup limits the distance of the closest approach between the target and the carbon foil (detection) to about 65 mm. The data show a pronounced modulation structure leading to the Fourier transform given in Fig. 9, where the frequency scale is based on a determination of the velocity v of scattered ions. The linewidth of the components of the transform is about 10 MHz and corresponds to the time interval of observation of about 120 ns. From the distribution of charge states (Fig. 3) we expect contributions from N I and N II terms. To isolate the components of hf splittings in N I, we apply an electric field behind the target and obtain the data shown in Fig. 10. The Fourier transform in Fig. 11 reveals only four frequency components. The results of the Zeeman beat experiments described in Sec. III, theoretical calculations [23], and the work of Radford and Evenson [11] imply that these components must be related to the hf splittings of the N I $2p^3\ ^2D$ term. The solid line in Fig. 10 represents a best fit to the data by

$$S/I(x) = \sum_i A_i \cos[\bar{\omega}_i(x+x_0)] \exp\left[-\left[\frac{\bar{\omega}_i(x+x_0)}{4} \frac{\delta v}{v} \right]^2 \Big/ \ln 2 \right] + (\text{constant background}) , \tag{6}$$

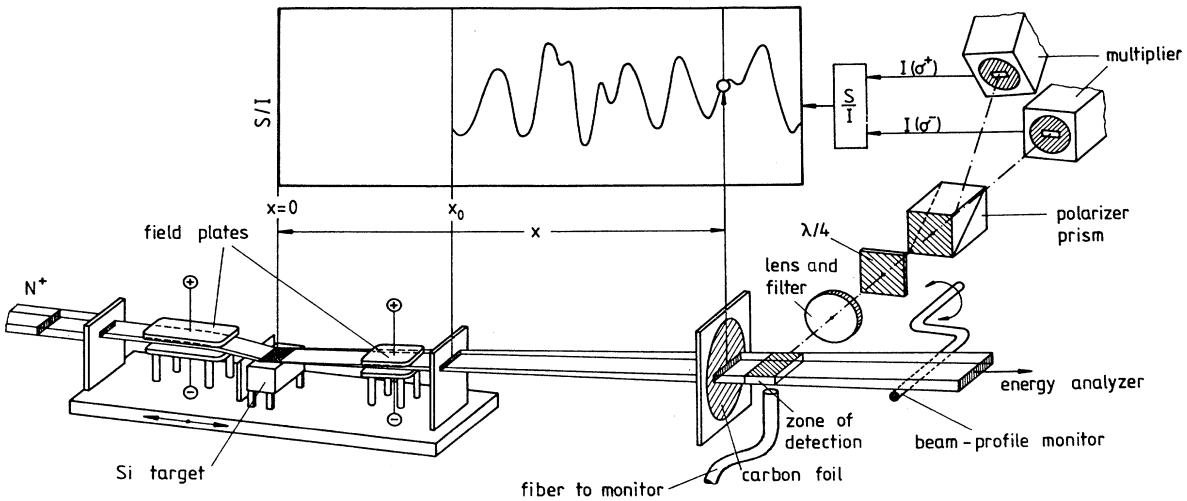

FIG. 7. Sketch of the setup and principle of measurement for a quantum-beat experiment.

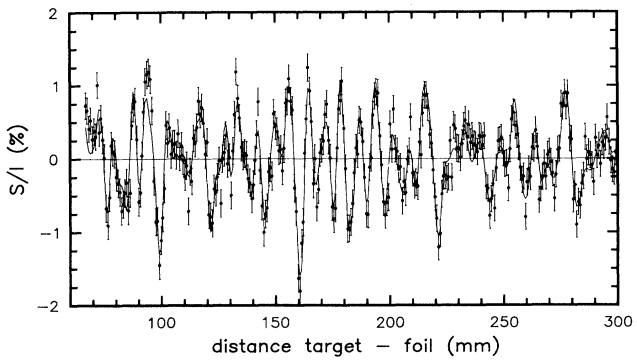

FIG. 8. Quantum-beat signal without charge state selection ($E_{in}=320$ keV; $\Phi_{in}=0.5°$; $\lambda_{det}=568$ nm; $\delta x=4.4$ mm).

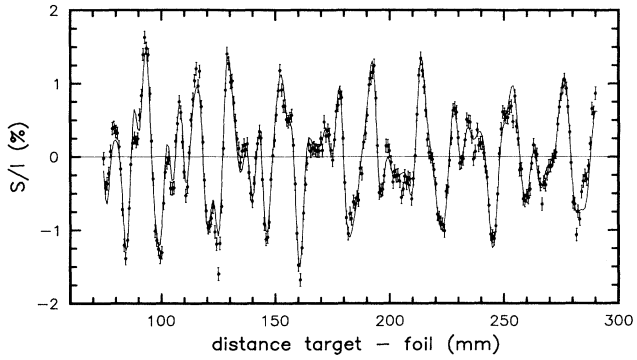

FIG. 10. Quantum-beat signal obtained for N I atoms ($E_{in}=300$ keV; $\Phi_{in}=0.5°$; "white-light detection"; $\delta x=4.4$ mm).

where $\bar{\omega}_i=\omega_i/v$, x_0 is the starting position of the measurement. The exponential term in Eq. (6) takes into account a damping of amplitudes due to the spread in velocity $\delta v/v$, neglecting a small asymmetry in energy straggling. In our experiment we find $\delta v/v\approx 0.01$, so that the reduction of amplitudes is generally small.

An interesting feature of the quantum-beat technique presented here is the possibility of a superposition of contributions from terms in different charge states. It was therefore intended to make use of the hf splittings in N I ^2D given by Rev. [11] (see Table II) as calibration standards. A relative comparison of our quantum-beat frequencies with the results obtained by Radford and Evenson [11], however, results in deviations from linearity. Due to this discrepancy we decided to establish an independent frequency calibration with a precise measurement of the velocity v of the scattered beam.

Figure 12 shows the energy distribution of 195-keV $^{14}N^+$ ions after scattering from a Si(111) surface at $\Phi_{in}=0.5°$ and an integral detection of the polar distribution of scattering. Tests with a horizontal slit (0.3 mm) in front of the entrance slit of the energy analyzer yield a variation of about 10^{-3} within the relevant part of the polar distribution of scattered ions. Energy loss and

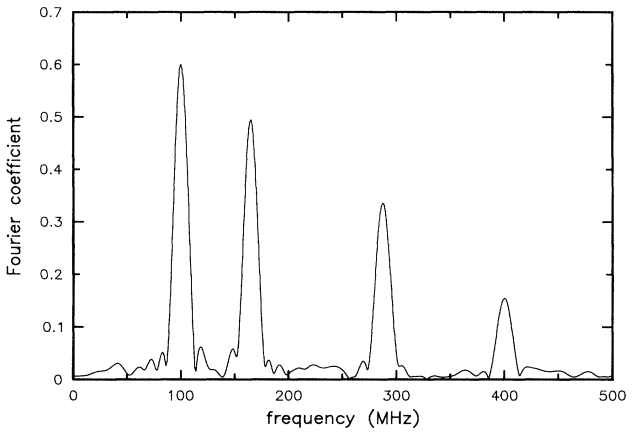

FIG. 11. Fourier transform of the data shown in Fig. 10.

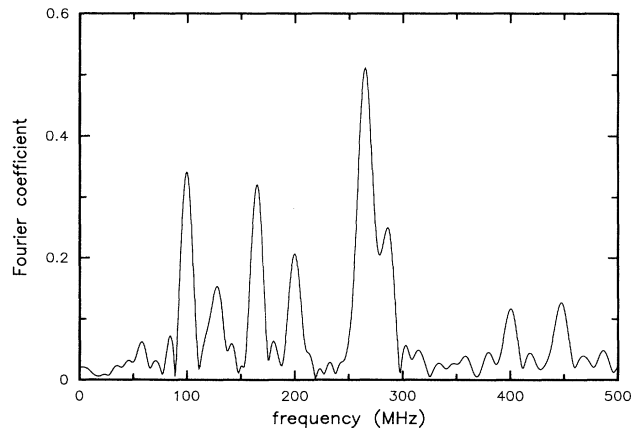

FIG. 9. Fourier transform of the data shown in Fig. 8.

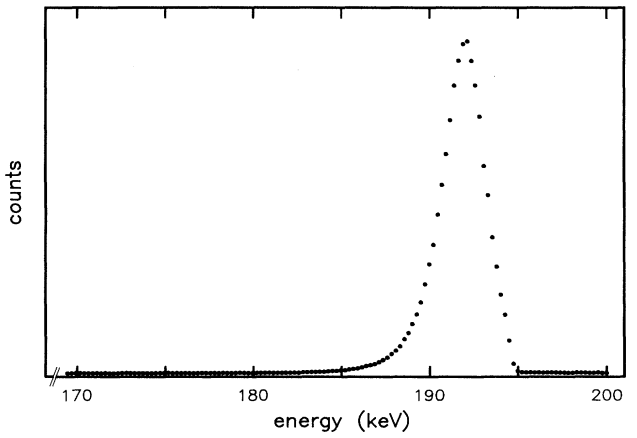

FIG. 12. Energy distribution of 195.1-keV $^{14}N^+$ ions after scattering from a Si surface under $\Phi_{in}=0.5°$.

TABLE II. Zero-field hf splittings in ^{14}N I $2p^3\,{}^2D_{3/2,5/2}$ obtained in measurements of Ref. [11] (a) and in our quantum-beat experiment (b).

^{14}N I $2p^3$	Splitting F_1-F_2	Frequency ν (MHz) (a)	(b)
$^2D_{5/2}$	$\frac{5}{2}-\frac{7}{2}$	401.00±0.33	400.88±0.28
	$\frac{3}{2}-\frac{5}{2}$	287.33±0.35	287.73±0.22
$^2D_{3/2}$	$\frac{3}{2}-\frac{5}{2}$	162.88±0.56	163.86±0.14
	$\frac{1}{2}-\frac{3}{2}$	98.63±0.54	99.08±0.10

straggling amount to about 1.5% of the projectile energy. The uncertainty of the mean energy is estimated conservatively to 50% of the FWHM of the energy distribution.

Table II gives the hf splittings of N I ^2D resulting from six independent runs. Comparison with Ref. [11] shows a discrepancy of about 1 MHz for the $J=\frac{3}{2}$, $F'=\frac{5}{2}-F=\frac{3}{2}$ splitting which is also confirmed by our rf experiments outlined in Sec. V. This discepancy and the lower precision of the splittings given in Ref. [11] led us to analyze our quantum-beat data for N II and N III on the basis of *our* evaluation for data for N I. We note that the splittings of N I ^2D obtained by the quantum-beat method are in excellent agreement with our rf experiments (see discussion in Sec. V).

The solid line in Fig. 8 represents a best fit to the data given by Eq. (6), where we have taken into account the hf splittings of all relevant terms in N I, II, III. The overall good description of data by the fit also gives consistent relative beat amplitudes of hf splittings of single terms deduced from Eqs. (2) and (4); the damping of amplitudes is consistent with an energy straggling of about 1.7% [see Eq. (6)].

In a number of experiments with $^{14}N^+$ projectiles with energies ranging from 140 to 300 keV, we investigated the hf splittings in N I, II, III, using the quantum-beat method and obtained the results given in Table III. Since the yield of N^{2+} ions at those beam energies is low, it was not possible to observe the splitting of N III $^2P_{3/2}$, $F'=\frac{5}{2}-F=\frac{3}{2}$ at about 250 MHz. Using a Van de Graaff accelerator (IPN, Lyon, France) we were able to increase the projectile energies up to 1.5 MeV for N_2^+ ions (molecular ions were used because of the beam intensity) which leads to a significant increase of the N^{2+} charge fraction. As an example Figs. 13 and 14 show data and the Fourier transform obtained by selective detection of the N III terms after the scattering of 1.1-MeV $^{14}N_2^+$ at $\Phi_{in}\approx 0.5°$. In both figures the two components of the hf splittings of N III $^2P_{3/2}$ are clearly identified. Experiment and results in N III have already been published elsewhere [12]; however, the hf splittings for N III given in Table III are obtained here by a reanalysis of data based on reference frequencies in N I, II with improved accuracy.

An analysis of our quantum-beat data shows that this technique is well suited for resolving hf splittings of stable terms with an accuracy of several 0.1 MHz. The range of frequencies that are accessible with the present setup is limited from a few 10 MHz up to about 500 MHz. We therefore did not succeed in resolving the hf splitting of N III $^2P_{1/2}$, which we expect to be at about 730 MHz. At very low frequencies the application of this technique also causes problems because the modulation period is comparable with the length of the data set and it is difficult to separate the signal from possible modulations of the background. By a selected detection of N II we found two frequency components at 4.5±0.5 MHz and 12.2±0.5 MHz. Based on theoretical studies (see Sec. VI) one may ascribe these splittings to N II $^3P_1$, but the status of experiment and analysis does not allow any definite statement to be made on these low-frequency components.

TABLE III. Results of quantum-beat measurements in N II and III (the data are calibrated by the hfs splittings of N I ^2D).

Zero-field splitting	Measurement by quantum beats (MHz)	Relative deviations to rf measurements (units of 10^{-4})
	^{14}N II $^3P_2$	
$F'=2-F=1$	201.18±0.24	+2.2
$F'=3-F=2$	275.75±0.50	+4.1
	^{14}N II $^1D_2$	
$F'=2-F=1$	264.73±0.21	+1.8
$F'=3-F=2$	447.30±0.37	−3.0
	^{14}N III $^2P_{3/2}$	
$F'=3/2-F=1/2$	126.23±0.38	−7.8
$F'=5/2-F=3/2$	252.29±0.62	−11.9

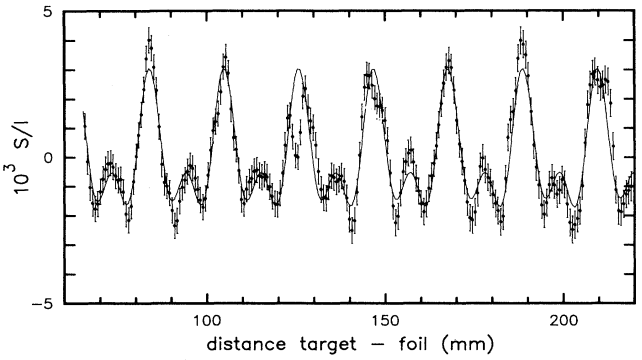

FIG. 13. Quantum-beat signal obtained with ^{14}N III ions after scattering of 1.1-MeV $^{14}N_2^+$ molecules from a Si surface under $\Phi_{in} \approx 0.5°$.

In the study demonstrating the feasibility of this quantum-beat technique on stable terms [3] extensive discussions of possible contributions to the data by excited terms via cascades can be found. It turned out, however, that in contrast to beam-foil excitation for example, grazing surface scattering results in a poor population of excited terms [2]. Since, in addition, the lifetimes of those terms are significantly smaller than the times of observation, an analysis on the influence of excited terms yields negligible contributions to our final results.

V. rf-RESONANCE EXPERIMENTS IN STABLE ATOMIC TERMS

The concept of our rf-resonance experiments is to modify the population of atomic hf levels after the surface scattering. In this way our method is similar to previous rf resonance studies using fast beams [13]. The modification through $M1$ transitions between levels $|LSJF_1M_1\rangle \equiv |F_1M_1\rangle$ and $|LSJF_2M_2\rangle \equiv |F_2M_2\rangle$ slightly alters the collision-induced anisotropy of the $|LSJ\rangle$ term and thus also the nuclear polarization P_I. Detection of P_I dependent on the rf frequency leads to a technique to resolve hf splittings in stable terms. Between excitation and detection we apply an oscillating magnetic field parallel to the y axis $H_y = H_0 \cos(\omega_{rf} t)$ of amplitude H_0 and frequency ω_{rf}. The probability of inducing transitions between $|F_1M_1\rangle$ and $|F_2M_2\rangle$ levels after an interaction time ΔT with the rf field is given by a Rabi-type expression [14]

$$P = \frac{\Omega_R^2}{(\omega_{JF_1F_2} - \omega_{rf})^2 + \Omega_R^2} \times \sin^2\left[\frac{\Delta T}{2}[(\omega_{JF_1F_2} - \omega_{rf})^2 + \Omega_R^2]^{1/2}\right] \quad (7)$$

with the averaged Rabi frequency [15]

$$\Omega_R = \left[\frac{J(J+1)(2J+1)(2F_2+1)}{3}\right]^{1/2} \times g_J \frac{\mu_B H_0}{\hbar} \begin{Bmatrix} F_1 & 1 & F_2 \\ J & I & J \end{Bmatrix}, \quad (8)$$

where $F_2 > F_1$ and $\Delta M = M_1 - M_2 = \pm 1$.

In order to provide an estimate of the signals in the experiment, in Fig. 15 we give relative level populations and relative transition probabilities of a $^3P_2$ term, $F_1 = 2 - F_2 = 3$. The level populations are obtained by assuming initial populations of orbital angular momentum sublevels $\sigma(LM_L) = \sigma(M_L)$: $\sigma(-1) = 0.5$, $\sigma(0) = 0.4$, $\sigma(1) = 0.1$, which results in an orientation parameter $P_L = -0.4$, a typical value after grazing incidence scattering.

From Fig. 15 and Eq. (7) it can be seen that interaction times ΔT in the microsecond regime are required to achieve a substantial change in population. Since, in addition, a number of further levels from different terms are not affected by the nonresonant rf field but contribute to the signal detected via P_I with a constant background, relative variations in S/I of 10^{-4}–10^{-3} are expected.

A. Experimental setup

The experimental setup of the rf resonance experiments has been partly described in Sec. III A and is shown in

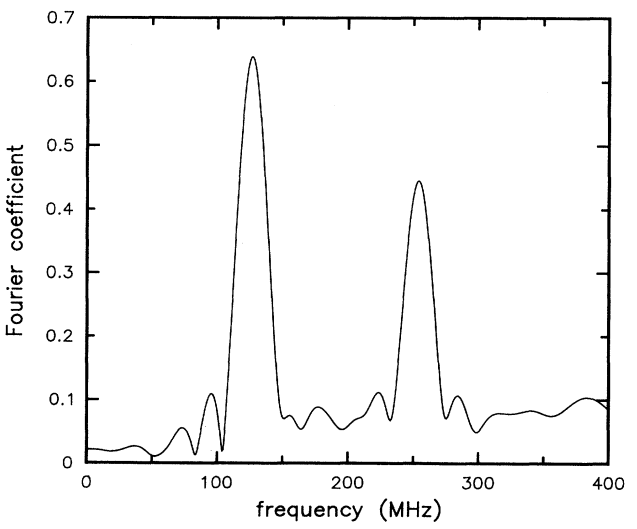

FIG. 14. Fourier transform of the data in Fig. 13.

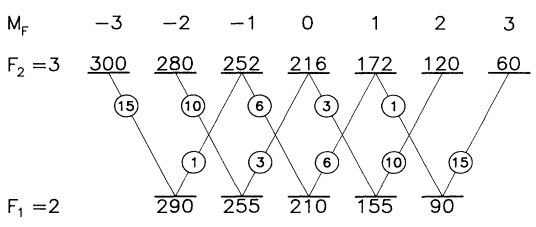

FIG. 15. Relative level population and transition probabilities for ($\Delta F = \pm 1$, $\Delta m_F = \pm 1$) transitions in a $^3P_2$ term ($F_1 = 2 - F_2 = 3$); model parameters are given in the text.

Fig. 1. The rf magnetic field H_y is generated by a coaxial transmission line 4 m in length made of copper tubes, the inner electrode 10 mm and the outer electrode 23 mm in diameter. The impedance of this wave guide is $Z=50\ \Omega$, and by terminating one end with a high-power Ohmic load of 50 Ω, voltage standing-wave ratios (VSWR) <1.4 for rf frequencies of up to 500 MHz are obtained. The rf was provided by a frequency synthesizer Marconi Model 2019A and a linear broadband amplifier ENI Model 525LA. rf powers of less than 30 W were used. A discharge in the wave guide triggered by the ion beam limits the rf power and field amplitudes H_0 in the experiments. The interaction time intervals ΔT result from the length of the wave guide of 4 m. Since the inner spacing of the two coaxial tubes is only about 6.5 mm, it is a difficult procedure to align the line along the path of the scattered beam. The interaction times $\Delta T<3.5$ μs and the rf powers available limit the Rabi frequencies to $\Delta\Omega_R<0.8$ MHz.

To monitor the small variations in S/I due to a resonance with the rf field, the method of detection must to a large extent eliminate any source of disturbance (beam fluctuations, modification of the carbon foils, etc.). It turns out that a simultaneous detection and gating of both optical channels is an essential prerequisite for a successful performance of the experiments.

B. Experiment and results

In the geometry of our experiment the rf wave propagates at about the speed of light $v_{rf}\approx c$ collinear with the beam axis. Thus frequencies ν_0 in the rest frame of the fast atoms moving with velocity v are shifted in the laboratory frame. These can be calculated from $\nu_0^2=\nu^+\nu^-$, where $\nu^\pm$ denotes the two cases for parallel and antiparallel propagation of the fast beam and the rf wave. The Doppler effect is eliminated by measurements of hf splittings in both directions of propagation [16].

To obtain larger S/I modulation signals we perform a selection of the charge states of the scattered projectiles by an electric field in the drift zone between the target and the transmission line. Contributions from atoms in a given charge state are then detected by tilting the transmission line and the detector at an angle to the beam axis. The inner spacing of the wave guide and the diameter of the foil holder (6 mm) limit the acceptance angle for scattered projectiles to about 1 mrad. Despite this extreme collimation, beam currents of up to several nanoamperes and counting rates of about 10^5 counts/s are observed after the beam-foil interaction.

Data obtained for N I are displayed in Figs. 16 and 17, where the variation of $\Delta S/I$ with rf frequency is plotted for antiparallel and parallel propagation of the rf wave with respect to the fast beam. The data were obtained at a projectile energy $E_0=100$ keV and the hf splittings of N I $^2D_{5/2}$, $F_1=\frac{5}{2}-F_2=\frac{7}{2}$ and N I $^2D_{3/2}$, $F_1=\frac{3}{2}-F_2=\frac{5}{2}$ were observed. The solid lines represent best fits to the data by Eq. (7) which give a satisfactory description of the line shape of the resonance signal. The data clearly reveal the expected Doppler shift of $\approx\pm4\times10^{-3}$. The experimental linewidth of 250 kHz is dominated by transit time broadening, which is expected to be $\delta\nu\approx0.85/\Delta T$ for these experiments. A direct comparison of the data in Fig. 17 and the hf splitting calculated from hf parameters reported by Ref. [11] [162.88(56) MHz] shows the discrepancy which has already arisen in the discussion of our quantum-beat data in Sec. IV. The intrinsic accuracy of the rf method allows us to conclude that the hf splitting of the N I ^2D term deduced from Ref. [11] is not as precise as regards the errors quoted by the authors. This explains our difficulties, reported in Sec. IV, in relating the hf splittings of N I ^2D given in Ref. [11] to our results.

For measurements in N II we show in Fig. 18(a) as a representative example data for N II $^1D_2$, $F_1=1-F_2=2$. The linewidth in the experiments obtained with N II is about 310 kHz due to $\Delta T=2.8$ μs. All hyperfine splittings in N II $^1D_2$ and N II $^3P_2$ are observed. We also tried to investigate N II $^3P_1$ and found a "resonant structure" at about 12.5 MHz. However, the quality and reproducibility of the data did not allow a reliable analysis. In order to obtain a sufficient fraction of N III ions in the scattered beam, we have to increase the beam energy to $E_0=350$ keV. The reduced transit time $\Delta T\approx1.9$ μs leads to a linewidth $\Delta\nu\approx470$ kHz. Figure 18(b) shows data for N III $^2P_{3/2}$, $F_1=\frac{1}{2}-F_2=\frac{3}{2}$. Both hf splittings of N III $^2P_{3/2}$ are observed. The hf splitting of N III $^2P_{1/2}$ is expected at a frequency about 730 MHz, which could not

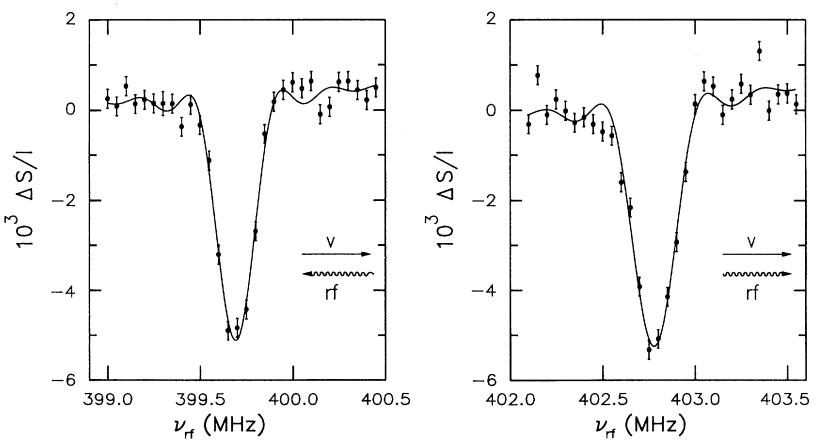

FIG. 16. rf-resonance signal of the ^{14}N I $^2D_{5/2}$, $F_1=\frac{5}{2}-F_2=\frac{7}{2}$ splitting detected via the nuclear polarization of the N I beam after scattering of 100-keV $^{14}N^+$ ions from a Si surface at $\Phi_{in}=0.5°$ ($\Omega_R=0.5$ MHz; $\Delta T=3.4$ μs; $\Delta\nu=253$ kHz). The variation of the degree of circular polarization $\Delta S/I$ is displayed as a function of the frequency of the rf wave. Left figure: counterpropagating rf wave and ion beam; right figure: parallel rf wave and ion beam. Note a Doppler shift between both data sets.

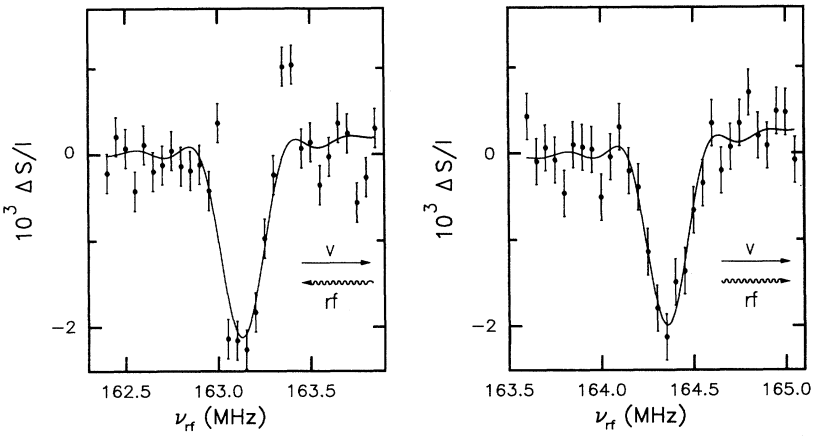

FIG. 17. rf-resonance signal of the ^{14}N I $^2D_{3/2}$, $F_1=\frac{3}{2}-F_2=\frac{5}{2}$ splitting detected via the nuclear polarization of the N I beam after scattering of 100-keV $^{14}N^+$ ions from a Si surface at $\Phi_{in}=0.5°$ ($\Omega_R=0.34$ MHz; $\Delta T=3.4$ μs; $\Delta\nu=256$ kHz). The variation of the degree of circular polarization $\Delta S/I$ is displayed as a function of the frequency of the rf wave. Left figure: counterpropagating rf wave and ion beam; right figure: parallel rf wave and ion beam.

TABLE IV. Results of measurements with our rf-resonance method. (a) Data obtained from the experiment. (b) Same as (a), but corrected for fine-structure perturbations.

Term	Hyperfine splitting $F'\leftrightarrow F$	Frequency (MHz) (a)	(b)
^{14}N I $^2D_{5/2}$	$\frac{7}{2}\leftrightarrow\frac{5}{2}$	401.227(28)	401.159(31)
	$\frac{5}{2}\leftrightarrow\frac{3}{2}$	287.751(20)	287.775(26)
^{14}N I $^2D_{3/2}$	$\frac{5}{2}\leftrightarrow\frac{3}{2}$	163.742(24)	163.718(29)
	$\frac{3}{2}\leftrightarrow\frac{1}{2}$	99.068(24)	99.024(26)
^{14}N II $^1D_2$	$3\leftrightarrow2$	447.438(56)	447.438(56)
	$2\leftrightarrow1$	264.682(32)	264.682(32)
^{14}N II $^3P_2$	$3\leftrightarrow2$	275.634(32)	275.646(32)
	$2\leftrightarrow1$	201.133(40)	201.129(40)
^{14}N III $^2P_{3/2}$	$\frac{5}{2}\leftrightarrow\frac{3}{2}$	252.592(28)	252.593(28)
	$\frac{3}{2}\leftrightarrow\frac{1}{2}$	126.331(28)	126.330(28)

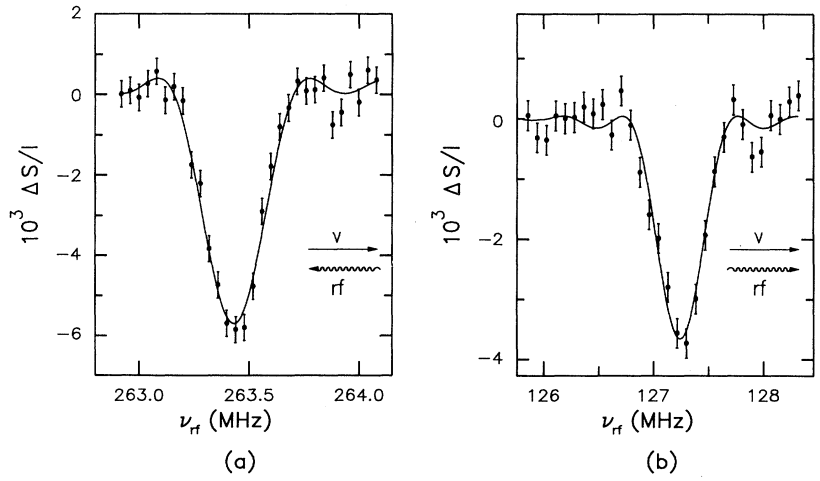

FIG. 18. (a) rf-resonance signal of the ^{14}N II $^1D_2$, $F_1=1-F_2=2$ splitting detected via the nuclear polarization of the N II beam after scattering of 150-keV $^{14}N^+$ ions from a Si surface at $\Phi_{in}=0.5°$ ($\Omega_R=0.64$ MHz; $\Delta T=2.8$ μs; $\Delta\nu=309$ kHz). The variation of the degree of circular polarization $\Delta S/I$ is displayed as a function of the frequency of the rf wave (counterpropagating to the ion beam). (b) rf-resonance signal of the ^{14}N III $^2P_{3/2}$, $F_1=\frac{1}{2}-F_2=\frac{3}{2}$ splitting detected via the nuclear polarization of the N III beam after scattering of 350-keV $^{14}N^+$ ions from a Si surface at $\Phi_{in}=0.5°$ ($\Omega_R=0.77$ MHz; $\Delta T=1.9$ μs; $\Delta\nu=466$ kHz). The variation of the degree of circular polarization $\Delta S/I$ is displayed as a function of the frequency of the rf wave (parallel to the ion beam).

TABLE V. List of contributions to the uncertainty in rf-resonance measurements in N II and N III (maximum observed errors are noted, all numbers are given in kilohertz). Row 1 shows the uncertainties of the center frequency as given by a fit according to Eq. (7), row 2 of the deviation from this if a background slope is allowed for. For the total energy stability, i.e., for the performance of the accelerator and the scattering from the surface, we regard as uncertainty a value of $\Delta E = 1$ keV for energies up to 150 keV and $\Delta E = 2$ keV for energies higher than 150 keV, a conservative assumption, as measurements of the long-time stability of surface scattering show. As the final error we give 4 times the maximum of rows 7 and 8 in order to include possible unknown systematics.

Source of error \ Resonance	447	264	275	201	252	126
Fit	11.2	4.5	12.5	8.6	8.7	13.1
Different background models	7.4	2.3	2.1	3.5	2.3	1.0
Total energy stability of ion beam	9.0	5.3	5.5	4.0	5.1	2.5
Variation of rf power over frequency interval	2.0	2.0	2.0	2.0	2.0	2.0
Calibration of rf generator	0.7	0.4	0.4	0.3	0.4	0.2
Number of independent runs	3	2	2	2	2	2
Mean error	8	5	8	10	7	7
Maximum deviation from mean frequency	14	8	6	10	4	7

be handled with our setup.

The results of the rf experiments are summarized in Table IV. At our level of precision second-order effects in hyperfine structure caused by interactions between fine-structure levels of the same configuration have to be taken into account. This small deviation of J from being a "good quantum number" introduces perturbative terms [17],

$$\delta(J,F)=\sum_{J'\,(\neq J)}\frac{|\langle IJFm_F|H_{\rm hyp}|IJ'Fm_F\rangle|^2}{W(J)-W(J')}\ , \tag{9}$$

with respect to the hf energies. In Table IV the experimentally observed hf frequencies and those corrected for fine-structure perturbations are given. The corresponding $\delta(J,F)$ have been calculated with configuration-interaction wave functions described below. The largest corrections of 40–70 kHz are deduced for levels in N I ^2D due to the small femtosecond splitting of 260.5 GHz [11]. As fine-structure intervals increase for more tightly bound ground term electrons in ionized nitrogen, second-order effects are reduced and amount to about 10 kHz for N II $^3P_2$, and less than 1 kHz for N III $^2P_{3/2}$. It should be noted that the N II $^1D_2$ term is not affected by the perturbations considered here.

The splittings in N II and N III given in Table IV have been determined for the first time; for N I our measurements improve the precision of former data (zero-field splittings) by factors of about 10–20 and remove an inconsistency in these data. The errors quoted in Table IV result from conservative estimates of possible sources of uncertainties in our experiments and do not exhibit the ultimate precision achievable with this method. In this respect it must be stressed that for each measurement of an hf component, more than 10^7 counts per channel have to be accumulated to analyze the small variation in S/I. This takes several hours and it is very time consuming to produce the larger number of independent runs needed for an analysis of data on the ultimate level of accuracy. Some sources of uncertainties are listed in Table V. At the present status in the deduction of nuclear moments from the data (see Sec. VI) there is no need to push the accuracy to the limits.

VI. THEORETICAL DESCRIPTION AND EVALUATION OF THE DATA

In this section we briefly discuss the theory of hyperfine interactions in free atoms and present results of self-consistent calculations of the hf splittings observed in our studies. We then deduce from theory and experiment the nuclear electric quadrupole moment $Q(^{14}\mathrm{N})$ and the quadrupole coupling constants $eQq_{\rm at}/h$. With respect to the theory of hyperfine interaction in free atoms we refer to the literature [17]. Magnetic dipole and electric quadrupole interactions result in corrections to the electronic energies [18],

$$\langle JIFM_F|H_m+H_Q|JIFM_F\rangle=E_m+E_Q$$
$$=\frac{1}{2}A_JK+B_J\frac{\frac{3}{4}K(K+1)-I(I+1)J(J+1)}{2I(2I-1)J(2J-1)} \tag{10}$$

TABLE VI. Comparison of experimental and theoretical hf parameters of stable terms in ^{14}N II and III. The left-hand side lists theoretical results in RHF and CI approach for single-electron parameters, which result in term-dependent A and B factors (values given in megahertz).

					b			Expt.	
Term	Method	a_1	a_{SD}	a_c	(20 mbar)	A_J	B_J	A_J	B_J
					^{14}N II $2p^2$				
$^1D_2$	RHF	144.25	0	0	17.602	144.25	14.082	144.105(14)	13.444(20)
	CI	143.42	0	0	16.808	143.42	13.446		
$^3P_2$	RHF	147.59	147.76	0	18.011	88.573	−7.204	94.487(10)	−6.946(18)
	CI	147.42	150.44	8.23	17.304	92.867	−6.921		
					^{14}N III $2p$				
$^2P_{3/2}$	RHF	180.09	180.30	0	21.977	96.022	8.791	96.833(10)	8.409(10)
	CI	179.91	190.54	1.256	20.940	94.950	8.376		

with $K=F(F+1)-J(J+1)-I(I+1)$. The interval factors A_J and B_J can be expressed in single-electron parameters a_k and b_k on the assumption of LS coupling.

In Table VI we give the single-electron parameters obtained in restricted Hartree-Fock (RHF) [19] calculations for terms with $2p$ and $2p^2$ configurations. We compare the calculated A_J and B_J with our experimental results where we use $Q(^{14}\text{N})=20.0$ mbarn (see Sec. VI A) to deduce the theoretical B factors. In order to take into account the polarization of the core by electrons of the open shell [20], we also perform calculations in a configuration-interaction (CI) approach by using the computer code CIV3 by Glass and Hibbert [21]. For light atoms, the effects of configuration interaction are relatively more important than relativistic effects [22]. In our calculations we take into account all one- and two-electron excitations allowed by symmetry up to the principle quantum number $n=4$. With these restrictions in excitations a successful description of hyperfine interaction in stable terms of other first row atoms has been obtained [23].

The RHF method provides an excellent description of A_J factors for $^1D_2$ and $^2P_{3/2}$, but for $^3P_2$ the deviation from the experimental results amounts to 6.3%. The experimental data for the B_J factors are reproduced within 5%. In the CI calculations the discrepancy with respect to the A_J factor of ^3P is largely removed. An inspection of the single-electron parameters a_k indicates that the rel-

TABLE VII. Variation of single-electron hf parameters for the ^{14}N $2p^2\,^3P$ term by inclusion of additional configurations with excited electronic orbitals to the wave function. All one- and two-electron excitations allowed by symmetry are taken into account up to $n=4$. The first row gives RHF parameters, with single-electron parameters resulting from one radial integral $\langle r^{-3}\rangle_{2p}$ and no contact term. An admixture of one- and two-electron excitations to the wave function results in different radial integrals for spin dipole (SD), orbital and quadrupole parts of hfs and a nonvanishing contact interaction. With the exception of the contact term the last row gives the relative difference of parameters in the RHF and the configuration-interaction approach. Note that for a_c, contributions from K-shell excitations are overcompensated by those of the L shell, a result which has already been reported on in the literature for ground terms in B, C, N, O, and F by Glass and Hibbert [23].

Excitation	a_c	a_{SD}	a_l	b
None (RHF)	0.000 00	147.764 26	147.592 97	18.0111
$1s\rightarrow ns$	−1.965 37	147.763 87	147.592 94	18.0111
$1s\rightarrow nd$	−1.515 66	150.301 65	147.594 59	18.0525
$2s\rightarrow ns$	7.429 52	150.182 13	147.594 63	18.0524
$2s\rightarrow nd$	7.711 54	150.510 80	147.439 86	18.0197
$2p\rightarrow np$	7.751 67	150.838 89	147.766 38	18.0595
$1s^2\rightarrow nl^2$	7.752 44	150.839 08	147.766 53	18.0588
$1s^2\rightarrow nlnl'$	7.752 42	150.839 08	147.766 53	18.0588
$1s2p\rightarrow nlnl'$	7.741 06	150.838 12	147.765 53	18.0587
$2s^2\rightarrow nl^2$	7.8882 39	150.792 62	147.737 31	17.3392
$2s^2\rightarrow nlnl'$	7.882 26	150.792 62	147.737 31	17.3392
$1s2s\rightarrow nl^2$	7.897 04	150.792 43	147.737 04	17.3392
$1s2s\rightarrow nlnl'$	7.897 00	150.792 43	147.737 00	17.3392
$2s2p\rightarrow nl'nl'$	8.228 41	150.441 59	147.416 72	17.3037
CI-RHF difference	8.228 41	+1.8%	−0.1%	−3.9%

atively large contact contribution introduced by CI mixing found in ^3P is the origin of the poor description of the hf interaction by RHF. In Table VII we list the variation of the single-electron parameters for ^3P for a successive number of CI excitations. In general A_J is reproduced for all three terms of better than 2%.

A striking feature of our CI calculations is an overall agreement of the theoretical B_J factors with the experiment of better than 0.4%. This consistent description of the quadrupole interaction in the ^{14}N II and ^{14}N III atoms is the basis of a determination of $Q(^{14}\mathrm{N})$ with improved accuracy (see Sec. VI A). We expect only small contributions from CI excitations into even higher electronic shells and into the continuum.

A. Nuclear electric quadrupole moment $Q(^{14}\mathrm{N})$

In the theoretical analysis of data in the preceding section the final results sensitively depend on the size of the nuclear moments. Whereas the magnetic moment of the ^{14}N nucleus is established with good precision [24], this does not apply to the electric quadrupole moment $Q(^{14}\mathrm{N})$. The electronic ground state $2p^3\,^4S$ of the ^{14}N I atom is almost spherically symmetric, and from the extremely small B factor [25] a determination of Q is not possible. As a consequence, $Q(^{14}\mathrm{N})$ has so far been obtained from experimental nuclear quadrupole coupling constants in molecules and recently also in ionized atoms with the help of the theoretical electric field gradient at the position of the ^{14}N nucleus. The lack of knowledge of precise geometrical structures and vibrational corrections in the case of molecules, and the use of higher symmetries makes calculations of field gradients more simple and reliable for atoms than for molecules [26].

A compilation of values for $Q(^{14}\mathrm{N})$ over the past decades reveals a gradual increase by about 30% [27], which reflects the problems and the progress in the computation of *ab initio* electric field gradients by multiconfiguration approaches, particularly in a variety of molecules containing ^{14}N nuclei. In Table VIII we give a summary of some representative values for $Q(^{14}\mathrm{N})$ so far proposed. The presumably most accurate moment listed here has been obtained in an analysis of hf splittings of an excited term in the ^{14}N II atom [37] by Scuseria and Schaefer [26].

The data presented here and our calculations form an excellent basis for deducing $Q(^{14}\mathrm{N})$ from N II and N III. Relating the single-electron parameters b_{nl} obtained from the measurements (B_J) to our CI calculations, i.e., using the theoretical values for the quadrupole radial parameters, we find $Q(^{14}\mathrm{N})$ as listed in Table IX. The errors of the theoretical analysis are difficult to estimate. At the current state of the evaluation we give increased weight to $Q(^{14}\mathrm{N})$ derived from the $^1D_2$ term, where the lack of spin-dependent contributions simplifies the analysis. In this analysis the discrepancies between experimental and calculated A factors must be taken into account, which have served as a guess of the theoretical uncertainties in the B factors. The resulting total uncertainties are listed in Table IX, where the final value for Q stems from the weighted mean of the individual evaluations. Note the good agreement of results for the quadrupole moment Q in the table, deduced from independent measurements in different atomic terms of two charge states. From our analysis we conclude that $Q(^{14}\mathrm{N})=20.0(2)$ mbarn. This value is in line with the results of recent evaluations as listed in Table VIII. However, we believe that our work has set a new "standard" in the knowledge of the nuclear quadrupole moment of ^{14}N by achieving a high level of consistency in the independent derivation from three different atomic terms. A more sophisticated theoretical analysis of data as outlined for the excited N II $2p3p\ ^1P_1$ term in Ref. [26] is expected to obtain $Q(^{14}\mathrm{N})$ with even higher accuracy.

TABLE VIII. List of representative values for the nuclear electric quadrupole moment of ^{14}N in past decades.

Q (mb)	Derived from	Year	Ref.
16(7)	NO	1960	[28]
15.6	"average" mol.	1968	[29]
16.6	"average" mol.	1969	[30]
14.9 and 15.8	NH_3	1971	[31]
16.7 and 17.5	NH_3	1972	[32]
21.6 and 22.0	NH_3	1972	[33]
16.3	NH_3	1973	[34]
17.4(2)	electron scattering	1974	[35]
15.0(1.6)	"average" mol.	1980	[36]
19.3(8)	N II $^1P_1$	1980	[37]
20.2	N_2	1980	[38]
16.7(3)	NH_3	1983	[39]
19.5	NH_3	1983	[40]
20.8	NH_3	1986	[27]
20.0	HCN	1986	[41]
20.5	NO^+, N_2	1986	[42]
20.7(4)	N II $^1P_1$	1987	[26]

TABLE IX. Nuclear electric quadrupole moment of ^{14}N deduced from a comparison of our experimental results and theoretical analysis based on the B factors given in Table VI.

Term	Factor	Q (mbarn)
^{14}N II $2p^2\ ^1D_2$	$B_2=0.8b_{2p}$	$Q=20.00\pm0.10$
^{14}N II $2p^2\ ^3P_2$	$B_2=-0.4b_{2p}$	$Q=20.07\pm0.36$
^{14}N III $2p\ ^2P_{3/2}$	$B_{3/2}=0.4b_{2p}$	$Q=20.08\pm0.44$
		$\bar{Q}_{\text{weighted}}=20.01\pm0.10$

B. Quadrupole coupling constant eQq_{at}/h

The electric quadrupole interaction can be used to study electronic configurations and structures of molecules. Townes and Daily [43] showed that the contributions of atomic field gradients q_{at} play a dominant role in the description of hf interactions in molecules, and they proposed a method for detailed studies of molecules. The application of this method refers to field gradients generated by atomic constituents of the molecules which dominate the quadrupole interaction, i.e., atoms in stable electronic configurations.

Studies of molecules containing ^{14}N atoms thus need information on the q_{at} of a single electron in the stable $2p^3\ ^4S$ term, given by the coupling constant eQq_{at}/h (^4S). Because of the very small field gradient q_{at} in the $2p^3$ configuration of the neutral ^{14}N atom, this coupling constant cannot be deduced directly from atomic data, and it is therefore derived from studies in different molecules with low precision. An evaluation of available experimental data can be found in the literature, where eQq_{at}/h (^4S)=10 MHz with about 20% uncertainty is reported [44]. O'Konski and Ha [45] derived the coupling constant from calculated field gradients in ^{14}N atoms and obtained 9.09 MHz. In this analysis the commonly accepted value at that time for the nuclear quadrupole moment $Q(^{14}\text{N})=15.6$ mbarn has been used (see Sec. VI A). Based on the concept discussed in Ref. [45], the coupling constant eQq_{at}/h in ^4S is deduced here from hf splittings in stable terms of N II and N III.

Our analysis is discussed with the help of Table X. First we calculate or take from the literature electric field gradients for ^{14}N III $2p\ ^2P_{3/2}$, ^{14}N II $2p^2\ ^3P_2$, and ^{14}N I $2p^3\ ^4S_{3/2}$. Then we compute the ratios of gradients in atoms with adjacent charge states which relate the corresponding coupling constants. These ratios are obtained from Ref. [45], RHF, CI, and MCDF (multiconfiguration Dirac-Fock) calculations [46]. The coupling constants for N III $^2P_{3/2}$ and N II $^3P_2$ are obtained directly from our experiments:

$$eQq_{2p}/h(2p\ ^2P_{3/2})=2B_{3/2}=16.818\pm0.040\ \text{MHz}\ ,$$

$$eQq_{2p}/h(2p^2\ ^3P_2)=-2B_2=13.892\pm0.036\ \text{MHz}\ .$$

As we have said, for atoms with $2p^3$ configurations this quantity cannot be determined by an experiment, and we therefore deduce this coupling constant by an extrapolation based on calculated ratios of field gradients. The analysis is started by taking the coupling constant for N III derived from our experiment and comparing the theoretical extrapolations for N II with the experiment (Table X). The agreement between theory and experiment is about 8×10^{-3} for RHF and within the experimental error of 2.6×10^{-3} for the multiconfiguration method. This may be interpreted to mean that ratios of electric field gradients in light atoms can be calculated with good precision. Extrapolation along the same lines for N I yields, as for N II, a slightly larger constant from MCDF compared with RHF, where we again expect the analysis based on MCDF to be more accurate and reliable.

At the present status of evaluation we give the conservative estimate for the quadrupole coupling constant in the ground term of N I: $eQq_{2p}/h(2p^3\ ^4S_{3/2})=11.2\pm0.2$ MHz, which significantly improves the knowledge of this constant. A more detailed discussion on this subject will be published elsewhere [47].

VII. CONCLUSION

We present two experimental techniques which allow hyperfine structures of stable terms to be resolved with

TABLE X. Quadrupole coupling constant for a single electron in the ground-state configuration of $^{14}N^{q+}$, $q=0,1,2$, obtained by different theoretical approaches and extrapolations. In the right-hand column we give the experimental results. For N I this constant cannot be deduced from experimental data.

	Theory				
State	RHF	Ref. [45]	CI	MCDF	Experiment
$2p\ ^2P_{3/2}$	16.818				16.818±0.040
↕	1.220 13	1.220 44	1.210 21	1.213 39	
$2p^2\ ^3P_2$	13.784	13.780	13.897	13.860	13.892±0.036
↕	1.236 96	1.236 26		1.234 54	
$2p^3\ ^4S_{3/2}$	11.143	11.147		11.227	

good precision. The potentials of the quantum beat and of the rf resonance technique have been demonstrated by investigating the hyperfine structures of different terms in three charge states of ^{14}N. The knowledge of hf interaction in stable terms of ^{14}N I, II, and III has been significantly improved by our studies. In combination with self-consistent atomic structure calculations it is possible to derive the nuclear quadrupole moment of ^{14}N and the nuclear quadrupole coupling constant for a single electron in the $2p^3$ configuration of the ground term in ^{14}N I.

The two techniques are time-of-flight methods. The quantum-beat method uses the frequency resolution gained with the fast beam by a variation of the distance between excitation and detection along the beam axis. In our experiments we vary this distance up to several hundred millimeters and with velocities in the mm/ns regime we therefore obtain observation times of several hundred nanoseconds. This results in corresponding linewidths of a few megahertz and uncertainties of about 10^{-3} to several 10^{-4} for the data. A higher frequency resolution is achieved with a new kind of rf resonance method, which can be regarded as an adaptation of the classic Rabi-type experiment for fast-beam surface scattering. The velocity of projectiles determines the time of interaction with the resonant rf field, which corresponds to the *C* region of the classic Rabi setup. The length of the wave guide used in our experiments provides times of interaction of several microseconds and linewidths of a few hundred kilohertz. Relative uncertainties of 10^{-4}–10^{-5} are easily obtained without going to the limits of the method.

Application of the rf method to higher charge states than those discussed here seem to be attractive for further atomic structure studies. In the *C* region a resonant laser field could then eventually be applied, which would expand the regime of frequencies applicable in this method. With the use of magnetized targets, where a polarization of atomic terms with vanishing orbital angular momentum is achieved by a capture of spin-polarized electrons, our method is also applicable then for investigations of *S* terms.

ACKNOWLEDGMENTS

The assistance of H.W. Ortjohann in the preparation of the experiments and of Dr. Y. Ouerdane (Lyon, St. Etienne) during the runs is gratefully acknowledged. We thank Dr. R. Silverans (KUL-Leuven) for his assistance and for providing a rf amplifier in an early stage of our investigations. This work has been supported by the Sonderforschungsbereich 216 (Bielefeld, Münster) and has been initiated by discussions with Dr. M. L. Gaillard (Orsay).

*Present address: PTB Braunschweig, Bundesallee 100, D-3300 Braunschweig, Federal Republic of Germany.

[1] H. G. Berry, L. J. Curtis, D. G. Ellis, and R. M. Schectman, Phys. Rev. Lett. **32**, 751 (1974); H. J. Andrä, Phys. Lett. **54A**, 315 (1975); N. H. Tolk, J. C. Tully, J. S. Kraus, W. Heiland, and S. H. Neff, Phys. Rev. Lett. **41**, 643 (1978).

[2] H. Winter and R. Zimny, in *Coherence in Atomic Collision Physics,* edited by H. Beyer *et al.* (Plenum, New York, 1988), p. 283.

[3] H. J. Andrä and H. Winter, Hyperfine Interact. **5**, 403 (1978).

[4] H. J. Andrä, H. J. Plöhn, R. Fröhling, and A. Gaupp, Z. Phys. A **281**, 15 (1977).

[5] H. Winter and R. Zimny, Hyperfine Interact. **22**, 237 (1985).

[6] H. Winter, M. Langheim, A. Schirmacher, R. Zimny, and H. J. Andrä, Phys. Rev. Lett. **52**, 1211 (1984).

[7] H. J. Andrä, in *Fast-Beam (Beam-Foil) Spectroscopy,* edited by W. Hanle and H. Kleinpoppen, Progress in Atomic Spectroscopy (Plenum, London, 1979), Pt. B.

[8] I. Martinson and A. Gaupp, Phys. Lett. Rep. C **15**, 113 (1974).

[9] W. Wittmann, Thesis, Freie Universität Berlin, 1978 (unpublished).

[10] R. M. Schectman, H. Fakhruddin, H. Winter, and A. Schirmacher, Nucl. Instrum. Methods, Phys. Res. Sect. B **31**, 253 (1988).

[11] H. E. Radford and K. M. Evenson, Phys. Rev. **168**, 70 (1968).

[12] A. Schirmacher, H. Winter, H. J. Andrä Y. Ouerdane, J. Desesquelles, G. DoCao, and A. Denis, J. Phys. (Paris) **48**, 905 (1987).

[13] S. D. Rosner, R. A. Holt, and T. D. Gaily, Phys. Rev. Lett. **35**, 785 (1975); W. J. Childs, Phys. Rep. C **211**, 113 (1992).

[14] N. F. Ramsey, *Molecular Beams* (Clarendon, Oxford, 1956).

[15] G. Borghs, P. de Bisschop, J. Odeurs, R. E. Silverans, and M. van Hove, Phys. Rev. A **31**, 1434 (1985).

[16] U. Nielsen, K. T. Cheng, H. Ludvigsen, and J. N. Xiao, Phys. Scr. **34**, 776 (1986).

[17] L. Armstrong, Jr., *Theory of Hyperfine Structure of Free Atoms,* (Wiley-Interscience, New York, 1971)].

[18] H. Kopfermann, *Nuclear Moments* (Academic, New York, 1958).

[19] C. Froese-Fischer, Comput. Phys. Commun. **4**, 107 (1972).

[20] R. M. Sternheimer, Phys. Rev. **80**, 102 (1950); Phys. Rev. A **6**, 1702 (1972).

[21] R. Glass and A. Hibbert, Comput. Phys. Commun. **11**, 125 (1976).

[22] A. Rosén, Phys. Scr. **8**, 159 (1973).

[23] H. F. Schaefer III and R. A. Klemm, Phys. Rev. **188**, 152 (1969); R. Glass and A. Hibbert, J. Phys. B **11**, 2257 (1978).

[24] Y. Ting and B. Williams, Phys. Rev. **89**, 595 (1953).

[25] S. B. Crampton, H. C. Berg, H. G. Robinson, and N. F. Ramsey, Phys. Rev. Lett. **24**, 195 (1970); J. M. Hirsch, G. H. Zimmerman III, D. J. Larson, and N. F. Ramsey, Phys. Rev. A **16**, 484 (1977).

[26] G. E. Scuseria and H. F. Schaefer, J. Chem. Phys. **87**, 4020 (1987).

[27] T. K. Ha, Z. Naturforsch. A **41**, 163 (1986).

[28] C. C. Lin, Phys. Rev. **119**, 1027 (1960).

[29] C. T. O'Konski and T. K. Ha, J. Chem. Phys. **49**, 5354 (1968).

[30] R. Bonaccorsi, E. Scrocco, and J. Tomasi, J. Chem. Phys. **50**, 2940 (1969).
[31] R. E. Kari and I. G. Csizmadia, Theor. Chim. Acta **22**, 1 (1971).
[32] E. A. Laws, R. M. Stevens, and W. N. Lipscomb, J. Chem. Phys. **56**, 2029 (1972).
[33] P. Grigolini and R. Moccia, J. Chem. Phys. **57**, 1369 (1972).
[34] J. D. Petke and J. L. Whitten, J. Chem. Phys. **59**, 4855 (1973).
[35] N. Ensllin, W. Bertozzi, S. Kowalski, C. P. Sargent, W. Turchinetz, C. F. Williamson, S. P. Fivozinsky, J. W. Lightbody, and S. Penner, Phys. Rev. C **9**, 1705 (1974).
[36] M. Barber, S. M. Hayne, and A. Hinchliffe, J. Mol. Struct. **62**, 207 (1980).
[37] H. Winter and H. J. Andrä, Phys. Rev. A **21**, 581 (1980).
[38] R. D. Amos, Mol. Phys. **39**, 1 (1980).
[39] J. W. Jost and C. T. O'Konski, J. Mol. Struct. **111**, 387 (1983).
[40] T. K. Ha, Chem. Phys. Lett. **107**, 117 (1983).
[41] G. E. Scuseria, T. J. Lee, R. J. Saykally, and H. F. Schaefer, J. Chem. Phys. **84**, 5711 (1986).
[42] D. Sundholm, P. Pyykko, L. Laaksonen, and A. J. Sadlej, Chem. Phys. Lett. **101**, 219 (1986).
[43] C. H. Townes and B. P. Dailey, J. Chem. Phys. **17**, 782 (1949).
[44] C. T. O'Konski, in *Determination of Organic Structures by Physical Methods,* edited by F. C. Nachod and W. D. Phillips (Academic, New York, 1962); E. A. C. Lucken, *Nuclear Quadrupole Coupling Constants* (Academic, New York, 1969); J. M. Lehn and J. P. Kitzinger, in *Nitrogen NMR,* edited by W. Witanowski and G. A. Webb (Plenum, London, 1973).
[45] C. T. O'Konski and T. K. Ha, J. Chem. Phys. **56**, 3169 (1972).
[46] B. Fricke (private communication).
[47] H. Winter, A. Schirmacher, and B. Fricke (unpublished).